A COMPARATIVE STUDY OF PLASMONIC EFFECTS IN ELECTROCHEMICALLY NANOSTRUCTURED $CuInS_2$ And $CuGaS_2$ CRYSTALS

V. V. Ursaki

Institute of Applied Physics of the Academy of Sciences of Moldova, Academiei str. 5, Chisinau MD-2028,
Republic of Moldova

(Received October 22, 2013)

Abstract

We investigate the differences in electrochemical nanostructuring of $CuInS_2$ and $CuGaS_2$ crystals. It is shown that thermal treatment of $CuInS_2$ crystals either in vacuum or in Zn vapors is a procedure providing necessary electrical conductivity to the as-grown high-resistivity crystals for a consequent electrochemical nanostructuring, while in $CuGaS_2$ crystals treatment in Zn vapors at temperatures higher than 700 ^oC is needed to make them suitable for electrochemical nanostructuring. Porous $CuInS_2$ structures with a uniform porosity and the pore diameter controlled by the crystal conductivity are demonstrated, while the porosity of $CuGaS_2$ structures is inhomogeneous. Possibilities of luminescence enhancement via thin Au and Cu film deposition onto nanostructured $CuGaS_2$ surfaces or ITO films onto $CuInS_2$ surfaces are also investigated.

1. Introduction

It has been demonstrated in previous works [1-3] that the surfaces of I-III-VI_2 ternary chalcopyrite materials can be nanostructured by electrochemical etching in aqueous electrolytes similarly to III-V [4–6] and II-VI [7–9] binary materials. However, there is an essential difference between electrochemical treatment of ternary and binary compounds. In contrast to binary compounds, anodization of ternary materials can be carried out only at low applied voltages of less than 1 V, since electrochemical treatment at higher voltages leads to the decomposition of these materials. The approach of electrochemical nanostructuring of semiconductors proves to be a strategy for a variety of applications. Particularly, the advent of methods for controlling inorganic materials on the nanometer scale opens new opportunities for the development of future generations of solar cells [10]. Solar cell technologies, using I–III–VI_2 direct band-gap chalcopyrite semiconductors as the absorber layer, have attracted great interest [11]. Solar cell technologies using I–III–VI_2 chalcopyrite semiconductors have made rapid progress in recent years. A conversion efficiency of around 20% has been reached with $Cu(In,Ga)Se_2$ thin-film solar cells [12, 13]. However, these solar cells contain a toxic component of Se. On the other hand, $CuInS_2$ does not contain toxic elements in comparison with $CuInSe_2$, while its band gap energy of about 1.5 eV matches well the solar spectrum for energy conversion, and it demonstrates a large absorption coefficient of 10^5 cm^{-1}. The advantages of nanostructured absorber layers in solar cells consist in trapping of light inside the cell instead of reflecting back out. Further boosting the performance of solar cells can be realized by combining nanostructuring with plasmonic effects by deposition of metallic nanostructures.

The goal of this paper is to perform a comparison of the effects of electrochemical

treatment upon $CuInS_2$ and $CuGaS_2$ crystals and to study the plasmonic effects in nanostructured layers of these materials covered with thin metallic films.

2. Sample preparation and experimental details

$CuInS_2$ and $CuGaS_2$ single crystals were grown by chemical vapor transport (CVT) in a closed system using iodine as a transport agent. The polycrystalline material, preliminary synthesized in iodine atmosphere from a stoichiometric mixture of the elemental constituents, was used as the raw charge in the CVT. The iodine concentration was approximately 5 mg cm^{-3}. The system was cooled down slowly at a rate of 10 °C/h to avoid straining of the crystals after crystal growth.

Electrochemical treatment for nanostructuring was performed in an electrochemical cell as described elsewhere [6]. A four Pt electrode configuration was used: a reference electrode in the electrolyte, a reference electrode on the sample, a counter electrode, and a working electrode. The area of the sample exposed to the electrolyte solution was 0.1 cm^2. The anodic etching was carried out in a 5% $HCl:H_2O$ electrolyte in the potentiostatic regime at room temperature. The resulting morphology of the etched samples was studied using a TESCAN scanning electron microscope (SEM). The photoluminescence (PL) was excited by a LD Pumped all-solid state MLL-III-532 laser, or by the 476.5 nm line of an Ar laser, and analyzed through a double spectrometer. The spectra were measured with a FEU 106 photomultiplier in a spectral range of 1.6–2.6 eV, with a FEU 62 photomultiplier in a spectral range of 1.1–1.6 eV, and with a PDA10DT InGaAs photodetector in a spectral range of 0.5–1.1 eV. The resolution was better than 1 meV. The samples were mounted on the cold station of a LTS-22-C-330 cryogenic system.

3. Results and discussions

The as-grown $CuInS_2$ and $CuGaS_2$ crystals are n-type with resistivity on the order of 10^6-10^7 Ω·cm and $>10^7$ Ω·cm, respectively. It is known that low resistivity crystals are required for nanostructuring by electrochemical treatment. For decreasing the resistivity of the as-grown $CuInS_2$ and $CuGaS_2$ crystals, a few types of thermal treatment have been applied. $CuInS_2$ crystals with the resistivity down to 0.3 Ω·cm were produced by annealing of crystals in vacuum. A similar treatment of $CuGaS_2$ crystals reduced their resistivity only to 10^4–10^5 Ω·cm. For a further decrease of resistivity, the samples were subjected to annealing in Zn vapors. The samples were subjected to annealing during 30 h. The parameters of samples as a function of the technological conditions are presented in Tables 1 and 2.

The PL spectrum of the as-grown grown $CuInS_2$ (sample #1) is presented by curve *1* in Fig. 1a. The spectrum consists of a few near-band-edge lines and a deeper PL band at 1.4 eV followed by unresolved phonon replicas. Among the near-band-edge lines, two most intensive lines at 1.52 and 1.53 eV are attributed to the recombination of bound excitons [14, 15], while the band at higher photon energies (1.537 eV) is due to the recombination of free excitons [14, 15]. The band at 1.4 eV was previously attributed to a free-to-bound optical transition with In interstitial (In_i) as a donor center involved in this transition.

Annealing of $CuInS_2$ crystals in vacuum at 700°C leads to the quenching of the exciton lines and the emergence of a new broad and asymmetric PL band in the near-band-edge region (at 1.55 eV). This PL band is attributed to the band-to-band transitions, since the shift of the

maximum and its broadening correlates with the shift of the equilibrium Fermi level [1–3]. A similar behavior was observed for the near-band-edge PL band in $CuInSe_2$ crystals subjected to a similar thermal treatment [2] and in ZnSe single crystals annealed in a Zn melt containing an Al impurity [16]. Note that the near-band-edge PL band is shifted to lower photon energies in samples annealed in Zn vapors as compared to samples annealed in vacuum [1, 2]. This behavior is explained in terms of the theory of heavily doped semiconductors [17, 18]. According to this theory, the asymmetric shape of PL bands is caused by potential fluctuations in the material due to the high concentrations of charged defects.

Table 1. Electrical parameters of $CuInS_2$ crystals subjected to different thermal treatment

$CuInS_2$	As grown, #1	Annealed in vacuum at 500°C, #2	Annealed in vacuum at 600°C, #3	Annealed in vacuum at 700°C, #4	Annealed in Zn vapors at 600°C, #5	Annealed in Zn vapors at 700°C, #6
ρ ($\Omega \cdot$ cm)	$10^6 \div 10^7$	20	1	0.3	0.1	0.05
n (cm^{-3})	-	$1 \cdot 10^{15}$	$3 \cdot 10^{16}$	$1.4 \cdot 10^{17}$	$6 \cdot 10^{17}$	$3 \cdot 10^{18}$
μ ($cm^2/V \cdot s$)	-	310	190	140	100	40

Table 2. Electrical parameters of $CuGaS_2$ crystals subjected to different thermal treatment

$CuGaS_2$	As grown, #1	Annealed in vacuum at 500°C, #2	Annealed in vacuum at 600°C, #3	Annealed in vacuum at 700°C, #4	Annealed in Zn vapors at 600°C, #5	Annealed in Zn vapors at 700°C, #6
ρ, ($\Omega \cdot$ cm)	$> 10^7$	$> 10^7$	$> 10^6$	$10^4 \div 10^5$	8	0.2
N, (cm^{-3})	-	-	-	-	$5.8 \cdot 10^{15}$	$3.3 \cdot 10^{17}$
μ, ($cm^2/V \cdot s$)	-	-	-	-	130	90

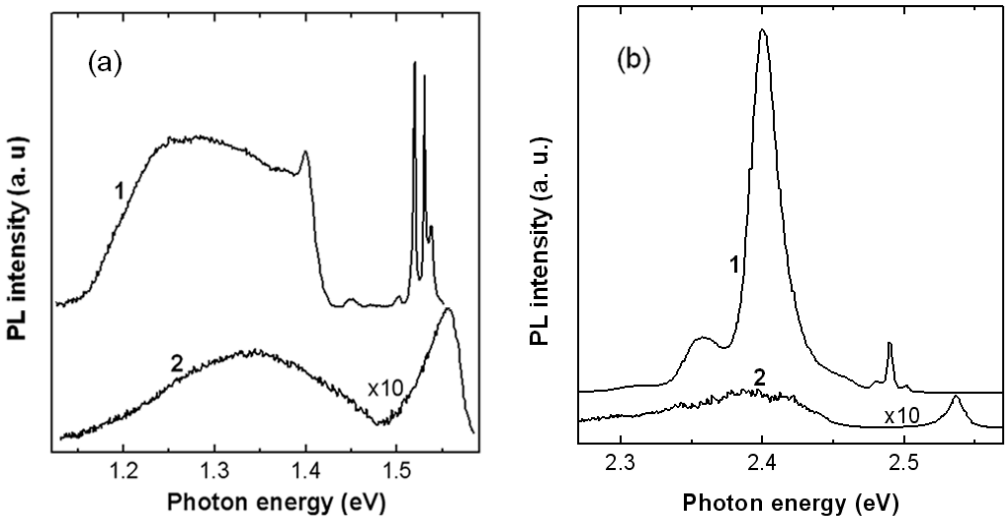

Fig. 1. (a) PL spectra of $CuInS_2$ crystals with numbers #1 (curve *1*) and #4 (curve *2*); (b) PL spectra of $CuGaS_2$ crystals with numbers #1 (curve *1*) and #6 (curve *2*). The spectra were measured at $T = 10$ K.

The PL spectrum of the as grown $CuGaS_2$ (sample #1) is presented by curve *1* in Fig. 1b. This spectrum is dominated by a strong PL band at 2.4 eV which has been previously attributed to donor acceptor pair (DAP) recombination [19, 20]. The weaker band at 2.357 eV is most probably a phonon replica of this DAP recombination. A series of three lines observed at higher photon energies is due to recombination of excitons. The line at 2.501 eV is due to recombination of free excitons [21]. The line at 2.490 eV is in the region of neutral donor bound exciton recombination [19, 22], while the band at 2.481 eV is in the region of excitons bound to neutral acceptors [21].

Unlike $CuInS_2$, annealing of $CuGaS_2$ crystals in vacuum at 700^{o}C or in Zn vapours at 600^{o}C leads only to a decrease in the luminescence intensity and broadening of the lines related to the recombination of bound excitons and to the disappearance of the band associated with the recombination of free excitons. At the same time, the spectrum of $CuGaS_2$ crystals annealed in Zn vapours at 700^{o}C (curve *2* in Fig 1b) resembles the spectrum of $CuInS_2$ crystals annealed in vacuum at 700^{o}C (curve *2* in Fig 1a). It consists of a PL band at 2.537 eV in addition to the PL band at 2.4 eV associated with the DAP recombination. That means that the high energy PL band (at 2.537 eV) in these samples is caused by potential fluctuations in the material due to the high doping.

The conductivity of $CuInS_2$ samples directly influences the processes of electrochemical etching. Porous layers with uniform porosity are produced under anodization with an applied voltage of 0.8 V in aqueous HCl electrolytes. The higher is the conductivity of the sample, the smaller is the pore diameter, which varies from 50 nm to 1 μm for porous layers produced on the basis of samples from Table 1. The morphology of a layer produced on $CuInS_2$ sample #4 is shown in Fig. 2.

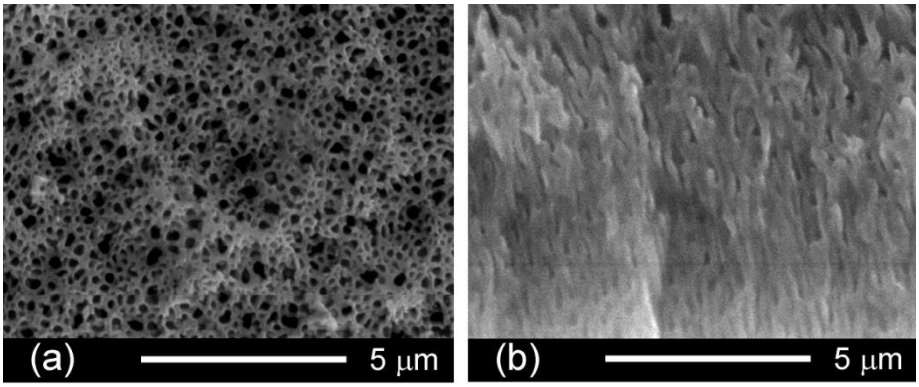

Fig. 2. Morphology of a porous layer produced on $CuInS_2$ sample #4 under anodization with an applied voltage of 0.8 V: (a) surface and (b) cross section.

Unlike $CuInS_2$, in $CuGaS_2$ crystals porosity can be introduced only in sample #6 from Table 2, since the conductivity of other samples is too low for the anodization. The morphology of the produced porous structure in this sample is non-uniform in comparison with $CuInS_2$ samples. One can see from Fig. 3a that the pore growth starts from separate regions *1* and *2*, and the pores propagate in radial directions as illustrated in Fig. 3b. When the pores propagating from regions *1* and *2* meet in region *4*, they further grow in the direction perpendicular to the initial sample surface, and a porosity illustrated in Fig. 3d is produced. At the same time, in isolated regions *3* the pores grow in a direction parallel to the sample surface, as illustrated in Fig. 3c.

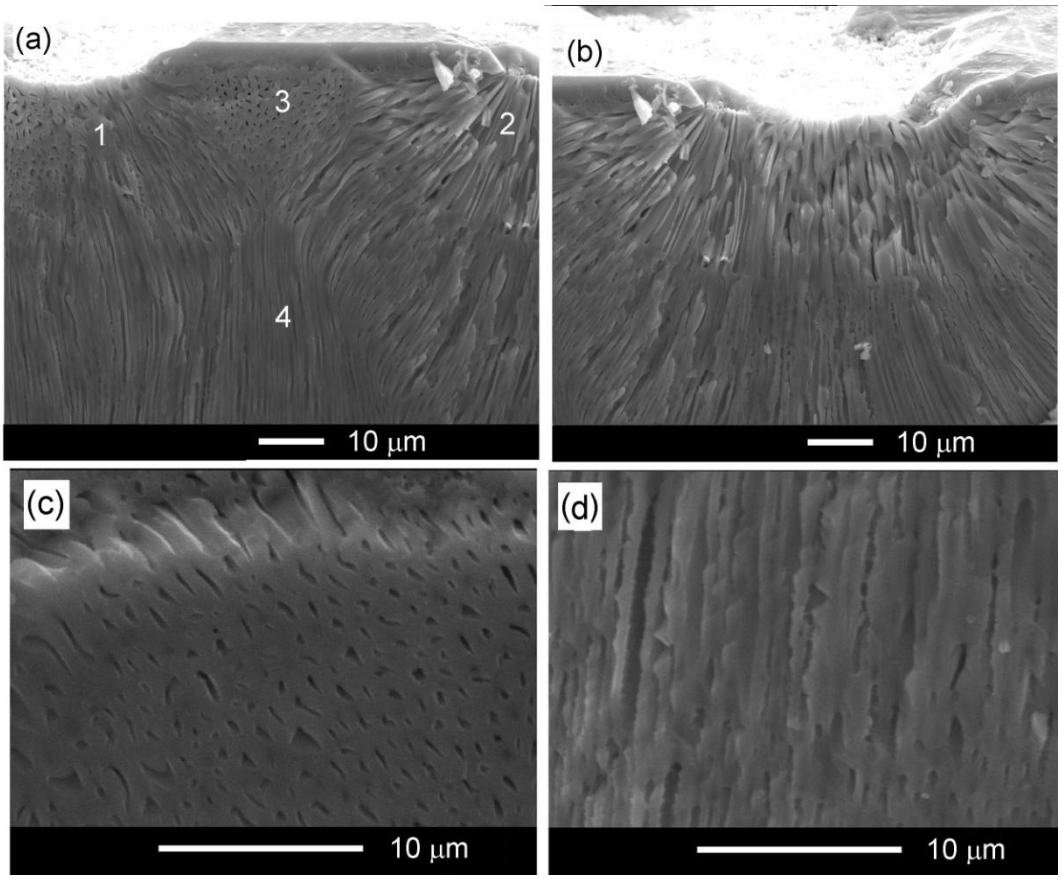

Fig. 3. (a) Morphology of a porous structure produced on $CuGaS_2$ sample #6 under anodization with an applied voltage of 0.7 V; (b) view of region *2*; (c) view of region *3*; and (d) view of region *4*.

Thin Au and Cu coatings were deposited onto nanostructured $CuGaS_2$ surfaces by means of a Cressington magnetron sputtering coater in order to investigate the plasmonic effects in metalized nanostructured ternary chalcogenides. Figure 4 illustrates the effect of deposition of thin Au and Cu films onto the surface of anodized $CuGaS_2$ sample #6. One can see that the integral PL spectrum of the as-anodized sample exhibits a PL band at 1.8 eV in addition to the above mentioned bands at 2.4 and 2.537 eV. A similar PL band was previously observed in Ga-rich $CuGaS_2$ layers [20].

One can see that deposition of thin Au films enhances the PL band at 2.4 eV and decreases the intensity of the 1.8 eV PL band. One can suggest that the enhancement of luminescence at 2.4 eV is due to surface plasmons, since the energy position of this PL band is close to the resonance energy of the surface plasmons at the $Au/CuGaS_2$ interface. On the other hand, the decrease of the intensity of the PL band at 1.8 eV is due to the absorption of the light in the metal film or due to the overall decrease of the PL intensity caused by the metal film deposition. The deposition of Cu films on the surface of the anodized $CuGaS_2$ sample, on the contrary, enhances the PL band at 1.8 eV and attenuates the PL band at 2.4 eV (Fig. 4b). That means that the resonance energy of the surface plasmons at the $Cu/CuGaS_2$ interface is closer to the position of the 1.8-eV PL band.

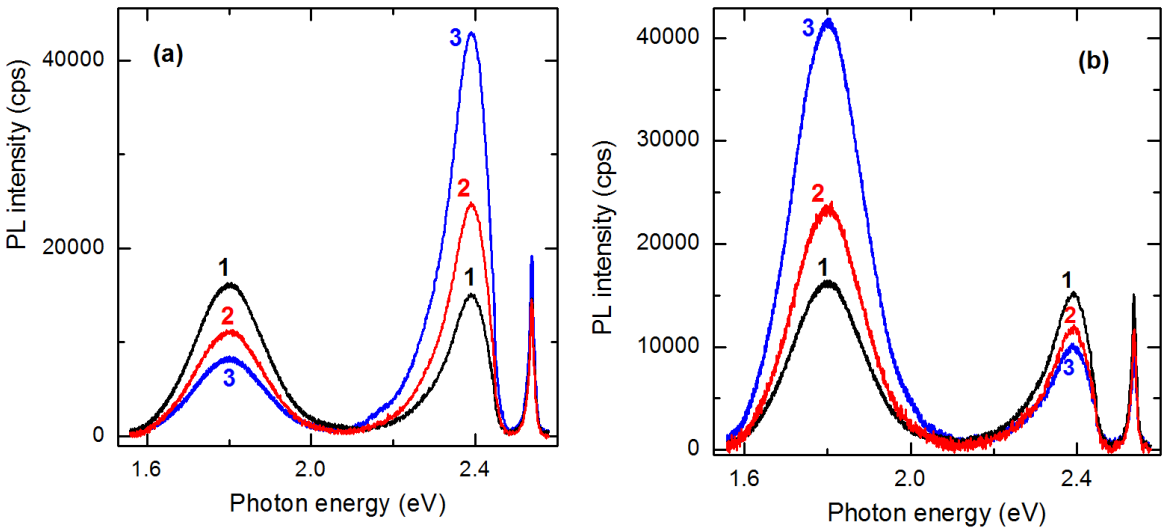

Fig. 4. (a) Low temperature (10 K) PL spectra of $CuGaS_2$ sample #6 after anodization (curve *1*), and after covering with Au films with a thickness of 5 (curve *2*) and 10 nm (curve *3*). (b) Low temperature (10 K) PL spectra of $CuGaS_2$ sample #6 after anodization (curve *1*) and after covering with Cu films with thickness of 5 (curve *2*) and 10 nm (curve *3*).

The influence of deposition of a conducting layer on the luminescence spectra was also investigated in porous $CuInS_2$ layers. No PL enhancement was observed after the deposition of Cu or Au films. On the contrary, the luminescence intensity decreased after the deposition of a metal film. An opposite effect was observed after the deposition of ITO films by a spray pyrolysis method described elsewhere [23]. Figure 5 shows the integral PL spectrum of nanostructured $CuInS_2$ sample #4. Several PL bands are observed in the low photon energy spectral interval in addition to the above mentioned bands at 1.3–1.4 and 1.55 eV.

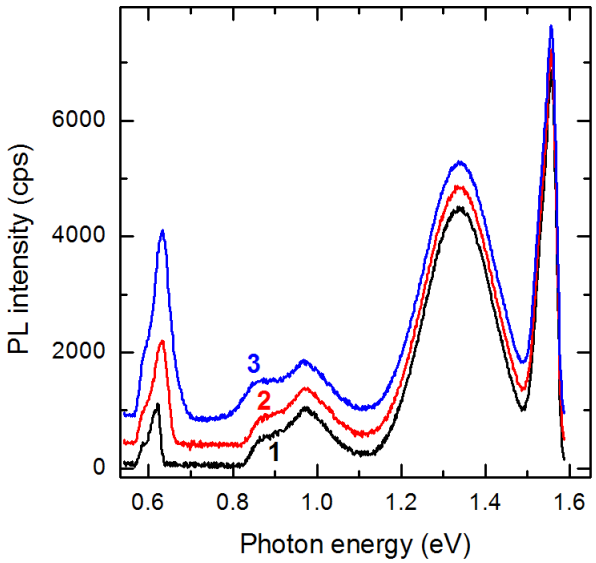

Fig. 5. Low temperature (10 K) PL spectra of $CuInS_2$ sample #4 after anodization (curve *1*) and after covering with ITO films with thickness of 5 (curve *2*) and 10 nm (curve *3*).

The PL bands at 0.87 and 0.97 eV have been previously assigned to the recombination within a deep-donor–deep-acceptor DD-DA complex. The underlying model was that these two bands are formed via a donor-acceptor pair recombination between pairs of the closest neighbors and between pairs of the next-closest neighbors, respectively [24]. The most long-wavelength band at 0.63 eV has been associated with a deep exciton bound to isoelectronic deep-donor–deep-acceptor pairs [24].

One can see from Fig. 5 that the infrared luminescence of the nanostructured $CuInS_2$ sample is enhanced by the thin ITO film deposition, and the luminescence intensity increases with an increase in the film thickness from 5 to 10 nm. The longer the wavelength of the PL band, the more prominent the luminescence enhancement. This effect suggests that the PL enhancement is again due to surface plasmons which exhibit a wide resonance at the ITO/$CuInS_2$ interface.

4. Conclusions

The results of this study demonstrate that porous $CuInS_2$ structures with a uniform porosity and the pore diameter controlled by the crystal conductivity can be produced by electrochemical treatment in an aqueous HCl containing electrolyte. The production of these structures is possible due to the control of the electrical resistivity in a range of 10^6–10^7 to 0.05 $\Omega \cdot$ cm by treatment either in vacuum or in Zn vapors at different temperatures. In contrast to this, only treatment in Zn vapors at temperatures above 700^{o}C provides a desired conductivity for $CuGaS_2$ crystals for the application of electrochemical nanostructuring, and the porosity of the structures produced in these crystals is non-uniform. A correlation exists between the material conductivity controlled by technological procedures and the photoluminescence spectra in both $CuInS_2$ and $CuGaS_2$ compounds. The luminescence of as-grown high-resistivity crystals is dominated by emission bands due to recombination of excitons and donor–acceptor pairs, while the near-bandgap PL spectra of highly doped crystals produced by annealing in Zn vapors at high temperatures consist of an emission band caused by potential fluctuations in the material due to the high concentrations of charged defects. The deposition of thin Cu films on nanostructured $CuGaS_2$ surfaces enhances the photoluminescence in a region of 1.8 eV, while Au films lead to the enhancement of luminescence in a region of 2.4 eV. Metallic coatings of Cu or Au have no positive effects on the photoluminescence of $CuInS_2$; on the contrary, the luminescence intensity is decreased by coatings. At the same time, the infrared luminescence of nanostructured $CuInS_2$ samples is enhanced by the deposition of a thin ITO film. These effects are attributed to the excitation of surface plasmons at the Cu/$CuGaS_2$, Au/$CuGaS_2$, or ITO/$CuInS_2$ interfaces.

Acknowledgments. This work was supported by the Academy of Sciences of Moldova, project 11.817.05.03A. The author would like to thank D. Sherban for the deposition of ITO coatings and M. Enachi for the deposition of metallic coatings on surfaces of the investigated samples.

References

[1] E. Monaico, V. Ursaki, V. Zalamai, A. Masnik, N. Syrbu, and A. Bullacu, Proc. 7th Int. Conf. Microelectron. Computer Sci., Chisinau, 2011, p. 139.
[2] V. V. Ursaki, Mold. J. Phys. Sci. 11, 312 (2012).
[3] V. V. Ursaki, Mold. J. Phys. Sci. to be published.
[4] H. Föll, S. Langa, J. Carstensen, M. Christophersen, and I. M. Tiginyanu, AdvanceMaterials, 15, 183 (2003).
[5] S. Langa, J. Carstensen, M. Christophersen, K. Steen, S. Frey, I. M. Tiginyanu, and H. Föll, J. Electrochem. Soc, 152 _8_ C525-C531 _2005.
[6] S. Langa, I. M. Tiginyanu, J. Carstensen, M. Christophrsen, and H. Föll, Appl. Phys. Lett., 82, 278 (2003).
[7] E. Monaico, V. V. Ursaki, A. Urbieta, P. Fernández, J. Piqueras, R. W. Boyd and I. M. Tiginyanu, Porosity induced gain of luminescence in CdSe. Semicond. Sci. and Technol. 19, L121-L123 (2004).
[8] I. M. Tiginyanu, E. Monaico, V. V. Ursaki, V. E. Tezlevan, and Robert W. Boyd, Appl. Phys. Lett. 86, 063115 (2005).
[9] E. Monaico, V. V. Ursaki, I. M. Tiginyanu, Z. Dashevsky, V. Kasiyan, and R. W. Boyd, J. Appl. Phys. 100, 053517 (2006).
[10] W. U. Hyunh, J. J. Dittmer, and A. P. Alivisatos, Science, 295, 2425 (2002).
[11] M. A. Green, K. Emery, D. L. King, S. Igari, and W. Warta, Prog. Photovoltaics 10, 355 (2003).
[12] M. Contreras, B. Egaas, K. Ramanathan, J. Hiltner, A. Swartzlander, F. Hasoon, and R. Noufi, Prog. Photovolt. 7, 311 (1999).
[13] I. Repins, M. A. Contreras, B. Egaas, C. DeHart, J. Scharf, C. L. Perkins, B. To, and R. Noufi, Prog. Photovoltaics 16, 235 (2008).
[14] I. H. Choi and D. H. Lee, Journal of the Korean Physical Society. 44, 1542 (2004).
[15] M. V. Yakushev, A. V. Mudryi, I. V. Victorov, J. Krustok, and E. Mellikov, Appl. Phys. Lett. 88, 011922 (2006).
[16] G. N. Ivanova, D. D. Nedeoglo, N. D. Nedeoglo, V. P. Sirkeli, I. M. Tiginyanu, and V. V. Ursaki. J. Appl. Phys. 101, 063543 (2007).
[17] A. P. Levanyuk and V. V. Osipov, Sov. Phys. Usp. 133, 427 (1981).
[18] B. I. Shklovskij and A. L. Efros, Electronic Properties of Doped Semiconductors, Springer, Berlin, 1984.
[19] S. Shirakata and S. Chichibu, J. Appl. Phys. 87, 3793 (2000).
[20] J. R. Botha, M. S. Branch, P. R. Berndt, A.W.R. Leitch, and J. Weber, Thin Solid Films, 6246 (2007).
[21] S. Levcenco, S. Doka, V. Tezlevan, D. Fuertes Marron, L Kulyuk, T. Schedel-Niedrig, M. Ch. Lux-Steiner, and E. Arushanov, Physica B 495, 3547 (2010).
[22] S. Shirakata, K. Saiki, and S. Isomura, J. Appl. Phys. 68, 291 (1990).
[23] A. Simashkevich, D. Serban, L. Bruc, A. Coval1, V. Fedorov, E. Bobeico, and Iu. Usatii, Mold. J. Phys. Sci. 3, 334 (2004).
[24] J. Krustok, J. Raudoja, and R. Jaaniso, Appl. Phys. Lett. 89, 051905 (2006).